Applied Catalysis B: Environmental 119–120 (2012) 74–80

Contents lists available at SciVerse ScienceDirect

Applied Catalysis B: Environmental

journal homepage: www.elsevier.com/locate/apcatb

Visible-light-activation of TiO_2 nanotube array by the molecular iron oxide surface modification

Yoshihiro Muramatsu, Qiliang Jin, Musashi Fujishima, Hiroaki Tada*

Department of Applied Chemistry, School of Science and Engineering, Kinki University, 3-4-1 Kowakae, Higashi-Osaka, Osaka 577-8502, Japan

ARTICLE INFO

Article history:
Received 9 December 2011
Received in revised form 14 February 2012
Accepted 17 February 2012
Available online 25 February 2012

Keywords:
TiO_2 nanotube array
Iron oxide
Surface modification
Visible-light-photocatalyst
Environmental purification

ABSTRACT

Uniform and adhesive TiO_2 nanotube arrays (TiO_2-NTAs) have been prepared by a two-step anodization in ethylene glycol solution containing NH_4F. The UV-light-activity of TiO_2-NTAs prepared by changing the electrolytic voltage and calcination temperature was studied for the degradation of 2-naphthol. Further, the surface of TiO_2-NTA has been modified with iron oxide species at a molecular scale by the chemisorption–calcination cycle technique. The iron oxide-surface modification endows TiO_2-NTA with a high level of visible-light-activity, concomitantly increasing the UV-light-activity. Under optimum conditions, the iron oxide-surface modified TiO_2-NTA exhibits a UV-light-activity comparable with that of highly active TiO_2 particles (P-25, Degussa).

1. Introduction

TiO_2-based photocatalyst is the most promising eco-catalyst for purification of polluted water and air [1,2]. The fundamental guideline for increasing the photocatalytic activity is the compatibility of high crystallinity and large surface area [3]. To satisfy this condition, nanometer-sized TiO_2 particles with a large surface area are frequently used in laboratory experiments. However, in the water remediation, the separation of TiO_2 particles from purified water is necessary. This cumbersome process becomes more difficult as the TiO_2 particle size decreases. Thus, from the practical viewpoint, supported TiO_2 catalysts are of great importance; however, the surface area of the usual TiO_2 film is quite small. Grimes and co-workers have originally developed an anodization process for preparing TiO_2 nanotube array (TiO_2-NTA) on the Ti plate [4–6]. The unique nanostructure of TiO_2-NTA renders it very attractive as a supported photocatalyst. First, it possesses a large surface area. Second, the one-dimensional (1D) open structure favors the diffusion of organic pollutants into the pores. Third, the very small wall thickness increases the probability for the photogenerated charge carriers to take part in the surface redox reactions. Forth, the TiO_2-NTA formed on Ti is regarded as a semiconductor–metal coupling system. For example, coupling TiO_2 with conducting fluorine-doped SnO_2 leads to a great increase in the photocatalytic activity of TiO_2 due to the enhancement of the charge separation through the interfacial electron transfer from TiO_2 to SnO_2 [7]. Fifth, TiO_2 and Ti are nonpoisonous. Due to these merits, a great deal of attention has been focused on the photocatalysis of TiO_2-NTAs. The photocatalytic activity should be checked for the substrate under the conditions where only TiO_2 is excited in order to exclude the degradation via the self-sensitization mechanism. Such studies on the photocatalysis of TiO_2-NTAs are only limited [8–10]. Another major problem of the TiO_2 photocatalyst is that it only responds to the UV-light occupying 3–4% of the incident sunlight. Even if high visible-light-activity can be obtained, it is usually much smaller than UV-light-activity. Then, to effectively use the sunlight, the compatibility of high visible-light-activity and UV-light-activity is important. For the visible-light-activation of TiO_2, doping of various transition metals and anions has extensively been studied, and reviewed in several papers [11–17]. Tang and Li have recently prepared sulfur-doped TiO_2-NTA by heating at 653 K under a H_2S flux [18]. The doping of TiO_2-NTA needs harsh chemical processes or physical high energy ones such as ion implantation and magnetron sputtering [11,19]. As the alternative, the visible-light-activation of TiO_2 can be achieved by the surface modification with iron oxides, which are harmless and abundance in nature, using the impregnation method [20,21] and the chemisorption–calcination-cycle (CCC) technique [22,23]. We have recently shown that the surface modification of TiO_2 particles (P-25, Degussa) having the highest level of photocatalytic activity among the commercial ones with molecular iron oxides by the CCC technique gives rise to a high level of visible-light-activity and a concomitant great increase in the UV-light-activity. This surface modification technique can be conveniently applied to TiO_2-NTA for its visible-light-activation.

* Corresponding author. Tel.: +81 6 6721 2332; fax: +81 6 6727 2024.
E-mail address: h-tada@apch.kidai.ac.jp (H. Tada).

0926-3373/$ – see front matter © 2012 Elsevier B.V. All rights reserved.
doi:10.1016/j.apcatb.2012.02.012

Here we show that iron oxide-surface modified TiO_2-NTA (FeO_x/TiO_2-NTA) prepared by the CCC technique is a promising supported photocatalyst for water purification. Under optimized conditions, it exhibits a high level of visible-light-activity and a UV-light-activity. To our knowledge, this is the first study on the application of the visible-light-active TiO_2-NTA to the degradation of model water pollutant excepting dyes, whereas an interesting study on the photoelectrochemical degradation of 4-chlorophenol using Cu_2O nanoparticle-loaded TiO_2-NTA as a photoanode has recently been reported [24].

2. Experimental methods

In order to prepare TiO_2-NTA with uniform pore size and shape, and strong adhesiveness, the 2-step anodization reported by Shin and Lee [25] was carried out. Titanium (Ti) plates (99%, 0.4 mm, Soekawa Chemicals) were used as the anode and cathode (25 mm × 40 mm). Ethylene glycol (EG) containing 0.5 wt% NH_4F was used as an electrolyte. Prior to the anodization, the Ti plates were cleaned by washing with acetone and distilled water. In the 1st-step anodization process, the Ti plate was anodized by applying an electrolytic voltage of 40 V between the electrodes using a dc-electric source (Kikusui Electronics) in the electrolyte solution for 0.5 h. The resulting film was removed by ultrasonic wave irradiation in distilled water. In the 2nd-anodization process, the resulting Ti plate was further anodized at a given voltage (U/V) for a given period (t_a/h). After washing with distilled water and dried, the sample was calcined at various temperatures (T_c/K) for 1 h. The sample was designated as TiO_2-NTA (U, t_a, T_c). The iron oxide-surface modification was carried out by the CCC technique in the same manner as reported in our previous papers [22,23]. The iron oxide species were too small to be observed by transmission electron microscopy (TEM). The amount of Fe loaded was expressed by the number of Fe ions per unit surface area of TiO_2-NTA (Γ/ions nm^{-2}) (Fig. 1).

The Fe loading amount was determined by inductively coupled plasma spectroscopy (ICPS-7500, Shimadzu). X-Ray diffraction (XRD) measurements were performed using Rigaku SmartLab with a thin film attachment. Scanning electron microscopic (SEM) observation was carried out by Hitachi S-4800 Type 2 at an applied voltage of 20 kV. TEM observation was performed using a JEOL JEM-3010 and Gatan Imaging Filter at an applied voltage of 300 kV. UV–vis diffuse reflectance spectra of TiO_2-NTAs were recorded on a Hitachi U-4000 spectrophotometer. The spectra were converted to the absorption spectra by using the Kubelka–Munk function. The photoluminescence (PL) spectra were measured with an excitation wavelength of 360 nm at 77 K using a JASCO FP-6000 spectrofluorometer. X-ray photoelectron spectroscopic (XPS) measurements were performed using a Kratos Axis Nova X-ray photoelectron spectrometer with a monochromated Al Kα X-ray source ($h\nu$ = 1486.6 eV) operated at 15 kV and 10 mA. The take-off angle was 90°, and multiplex spectra were obtained for F_{1s}, O_{1s}, and Ti_{2p} photopeaks. All the binding energies (E_B) were referenced with respect to the C_{1s} at 284.6 eV.

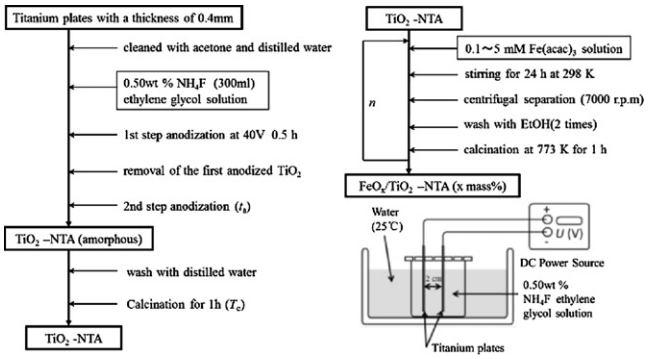

Fig. 1. Experimental procedures for preparing iron oxide-modified TiO_2-NTA.

In the decompositions of 2-naphthol (2-NAP), the reaction cells were irradiated with a Xe lamp (Wacom XRD-501SW) through a band-pass filter (D33S, AGC Techno Glass) superposed on a piece of FTO-coated glass transmitting only the 330–400 nm range for the UV-light photocatalytic activity evaluation (330 nm < λ < 400 nm, $I_{320-400\,nm}$ = 1 mW cm^{-2}) and a high pass filter (L-42, Toshiba) to cut off UV-light for the visible-light-induced activity test

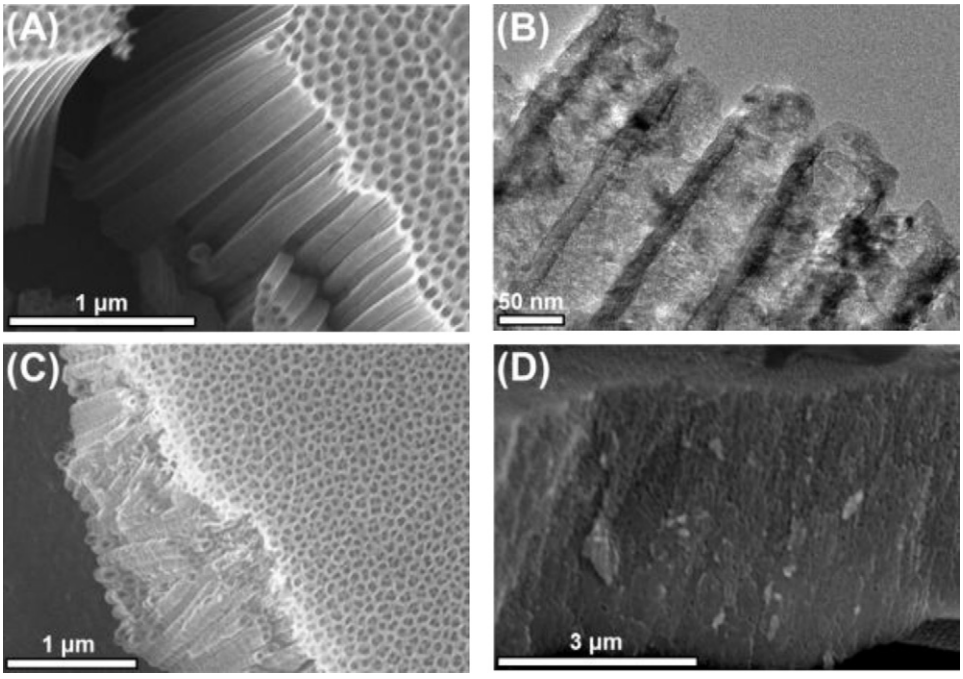

Fig. 2. SEM (A, C and D) and TEM (B) images of TiO_2-NTA (U = 40 V, t_a = 1 h, T_c): (A and B) T_c = 773 K, (C) T_c = 873 K, and (D) T_c = 1073 K.

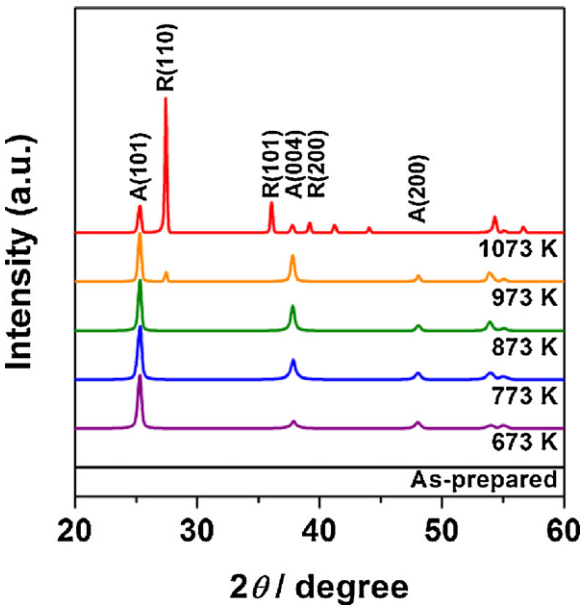

Fig. 3. XRD patterns of TiO_2-NTAs (U = 40 V, t_a = 1 h, T_c).

($\lambda > 400$ nm, $I_{420-485\,nm} = 3.0\,mW\,cm^{-2}$). TiO_2-NTA or FeO_x/TiO_2-NTA plates (25 mm × 40 mm) was placed in 50 mL of 1.0×10^{-5} M solution of 2-NAP (solvent, acetonitrile:water = 1:99, v/v) in a borosilicate glass container was irradiated with stirring. Two mL of the solution was sampled every 15 min and the electronic absorption spectra of the reaction solutions were measured using a spectrometer (Shimadzu, UV-1800) to determine 2-NAP concentration from the absorption peak at 224 nm.

3. Results and discussion

SEM (A, C and D) and TEM (B) images of the samples with varying T_c are shown in Fig. 2: (A and B) T_c = 773 K, (C) T_c = 873 K, and (D) T_c = 1073 K. At T_c = 773 K, regularly arrayed nanotubes with a mean pore size of 64 nm and length of 2.7 μm are formed on the Ti plate. The NTA structure observed at $T_c \leq 873$ K is lost by sintering at T_c = 1073 K. Table 1 summarizes the mean pore size and specific surface area of TiO_2-NTA (U = 40 V, t_a = 1 h, T_c). TiO_2-NTA (U = 40 V, t_a = 1 h, T_c = 673 K) has a large specific surface area (S_{BET}) of 45.6 $m^2\,g^{-1}$, which is comparable with the value for TiO_2 nanoparticles. Also, the S_{BET} is near the value calculated for a close packed model NTA with a hexagonal unit cell having a pore size of 60 nm, a wall thickness of 10 nm, and a length of 6 μm (34.1 $m^2\,g^{-1}$). Also, the roughness factor defined as the real surface area divided by the apparent surface area reaches ~270 for the model. The S_{BET} value monotonically decreases with an increase in T_c, whereas the pore diameter is almost maintained at ~60 nm in the range of 673 K ≤ T_c ≤ 973 K. The decrease in the S_{BET} can be attributed to the partial collapse of the nanotube structure with increasing T_c, which was confirmed by the SEM observation.

Fig. 3 shows XRD patterns of TiO_2-NTA (U = 40 V, t_a = 1 h) with varying T_c. The amorphous as-grown sample crystallizes as anatase at T_c = 673 K. As the T_c increases, the diffraction peaks become sharp at 673 K ≤ T_c ≤ 873 K. The mean size of anatase crystallites was determined by the Hall method [26]. As shown in Table 1, the crystallite size increases with an increase in T_c, which indicates that the crystallinity increases in this T_c range [3]. At T_c = 973 K, the phase transition from anatase to rutile starts, and the sample with T_c = 1073 K mainly consists of rutile phase. Fig. 4A shows plots of the mean pore size and wall thickness of TiO_2-NTA (U, t_a = 1 h, T_c = 873 K) vs. U. On increasing U, the pore size linearly increases,

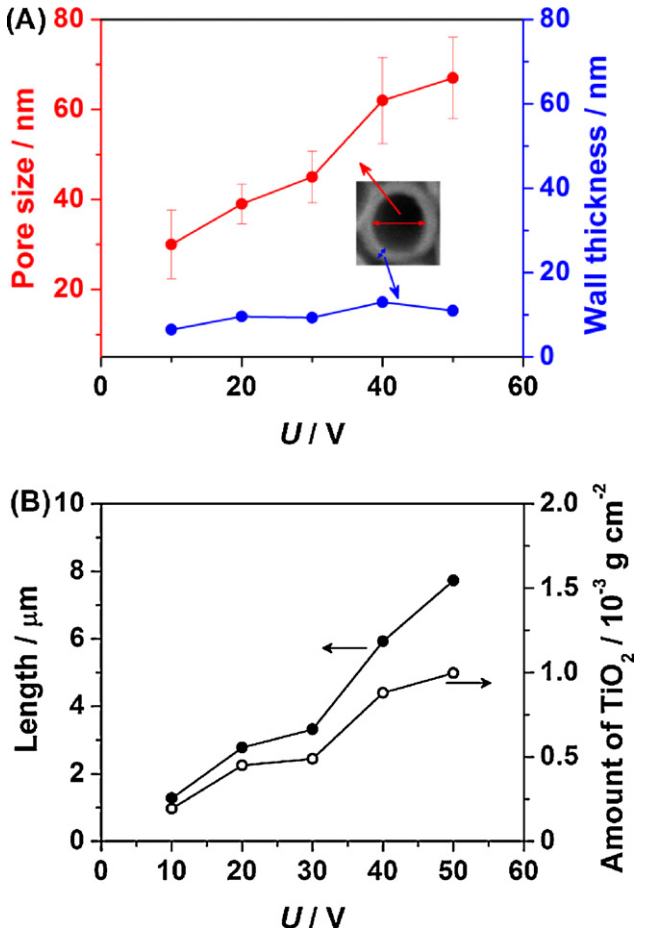

Fig. 4. (A) Plots of mean pore size and wall thickness of TiO_2-NTA (U, t_a = 1 h, T_c = 873 K) vs. U. (B) Mean nanotube length of TiO_2-NTA (U = 40 V, t_a = 1 h, T_c = 873 K) as a function of U.

whereas the wall thickness is almost constant at ~10 nm. Fig. 4B shows plots of nanotube length TiO_2-NTA (U, t_a = 1 h, T_c = 873 K) and the amount of TiO_2 vs. U. The amount of TiO_2 was calculated for a hexagonally packed model NTA using the pore size and wall thickness presented in Fig. 4A. The growth of the nanotubes is greatly enhanced with an increase in U, and the nanotube length at t_a = 1 h is almost proportional to U. Evidently, the pore size and length of TiO_2-NTA can be controlled in the ranges of 30–70 nm and 1–8 μm, respectively, by the electric voltage in the second anodization process.

To evaluate the photocatalytic activities of TiO_2-NTAs, the photocatalytic degradation of 2-naphthol (2-NAP) was carried out under illumination of UV-light (330 nm < λ < 400 nm, $I_{320-400\,nm} = 1.0\,mW\,cm^{-2}$). 2-NAP, the starting material of azo-dyes, is a suitable model water pollutant since it has no absorption at λ > 330 nm. Fig. 5A shows time courses for the TiO_2-NTA (U = 40 V t_a = 1 h, T_c)-photocatalyzed degradation of 2-NAP. Under the irradiation conditions, only TiO_2-NTA is excited, and UV-light irradiation of TiO_2-NTA was required to cause the degradation. The as-grown sample is almost inactive. The photocatalytic activity of amorphous TiO_2 is known to be small due to the recombination of the electron–hole pairs through bulk and surface defects [27]. In the systems with the post-heated TiO_2-NTA, the 2-NAP concentration decreases with increasing irradiation time (t_p) and the degradation rate strongly depends on T_c. Fig. 5B shows plots of $\ln(C_0/C)$ vs. t_p: C_0 and C denote the concentrations of 2-NAP at t_p = 0 and $t_p = t$, respectively. In every reaction system, the 2-NAP degradation apparently follows the first-order kinetics. The pseudo first-order

Table 1
BET surface areas, mean crystallite size, and mean pore size of TiO_2-NTA with varying T_c.

T_c/K	673	773	873	973	1073
BET surface, area/m^2 g^{-1}	45.6	42.7	31.4	27.7	16.3
Pore size/nm	61	61	62	64	–
Crystalline size/nm	14.2(A)	20.8(A)	35.9(A)	32.3(A), 37.3(R)	31.4(A), 41.3(R)

rate constant (k_{UV}) calculated from the slope of the straight line was used as an indicator for the photocatalytic activity. As shown in Fig. 6A, the k_{UV} value slightly increases with increasing T_c at 673 K ≤ T_c ≤ 873 K, significantly decreasing at T_c ≥ 973 K. The high photocatalytic activity of the samples with 673 K ≤ T_c ≤ 873 K can be achieved by the balance between the high crystallinity and the large specific surface area of anatase TiO_2-NTA. The significant lowering in k_{UV} at T_c > 973 K is mainly ascribable to the decrease in the S_{BET}. The phase transition from anatase to rutile can also be responsible for the very low activity of the sample with T_c = 1073 K because rutile shows a lower activity than anatase for the degradation of organics [28,29]. Fig. 6B shows the *U*-dependence of k_{UV} for TiO_2-NTA (*U*, t_a = 1 h, T_c = 873 K) indicating the increase in k_{UV} almost proportional to *U*. This increase in the k_{UV} well corresponds to the growth of the TiO_2-NTA with increasing *U* (Fig. 4B). This finding suggests that the smooth diffusion of 2-NAP into the 1D pores of TiO_2-NTA enables the reaction at the whole inner surfaces. The maximum k_{UV} of 0.40 h^{-1} is obtained for the TiO_2-NTA (*U* = 50 V). The UV-light-activity of TiO_2-NTA for the phenol degradation has been shown to further increase by loading Pt nanoparticles [8]. Also, phosphate-modified TiO_2-NTA has been reported to show a very high UV-light-activity for the decomposition of acetaldehyde [9].

Next, the visible-light-activation of TiO_2-NTA by the iron oxide-surface modification is described. The Langmuir type adsorption isotherm was observed for the adsorption of $Fe(acac)_3$ on the TiO_2-NTA surfaces. From the Langmuir plot, the saturated adsorption amount and adsorption equilibrium constant were calculated to be 1.79 ions nm^{-2} and 4.40 × 10^3 M^{-1}, respectively. Optical properties for FeO_x/TiO_2-NTA are of primary importance in connection with the photocatalytic activity. FeO_x/TiO_2 particles prepared by the conventional impregnation method using a precursor such as $FeCl_3$ have commonly a weak electronic absorption around 470 nm in addition to the absorption near 410 nm [30–33]. The former and latter absorption bands were attributed to the *d*–*d* transition and to the electronic transition from Fe^{3+} levels to the conduction band (CB) of TiO_2, respectively [34]. Fig. 7 shows UV–vis absorption spectra of FeO_x/TiO_2-NTA (*U* = 40 V, t_a = 1 h, T_c = 873 K) with varying Fe loading amount: $F(R_\infty)$ denotes the Kubelka–Munk function. Noticeably, the band gap narrowing occurs, while the

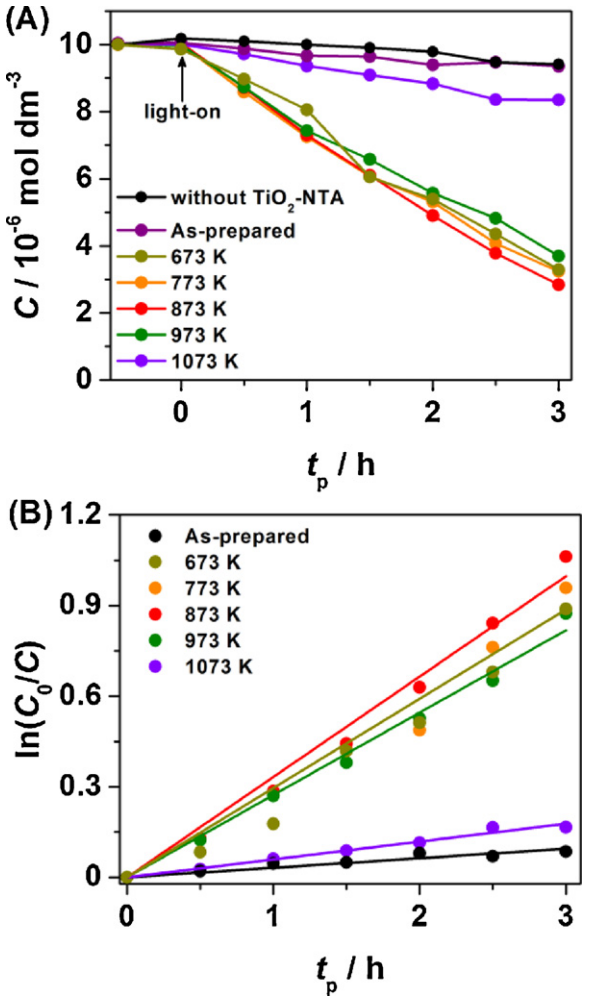

Fig. 5. (A) Time courses for the TiO_2-NTA-photocatalzyed degradation of 2-NAP. (B) Plots of $\ln(C_0/C)$ vs. t_p.

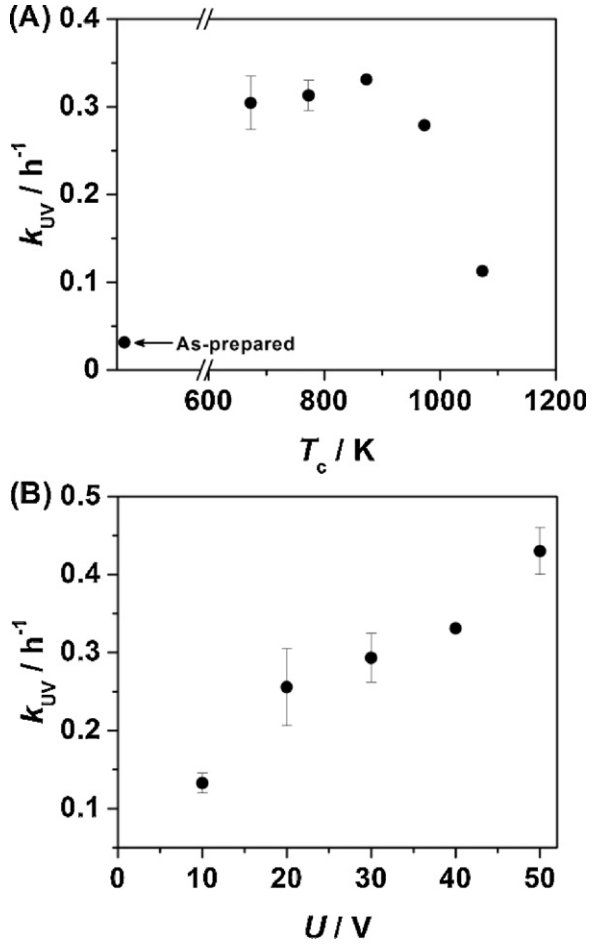

Fig. 6. (A) Plots of k_{UV} vs. T_c for the TiO_2-NTA-photocatalzyed degradation of 2-NAP. (B) Plots of k_{UV} vs. electrolytic voltage for the TiO_2-NTA-photocatalzyed degradation of 2-NAP.

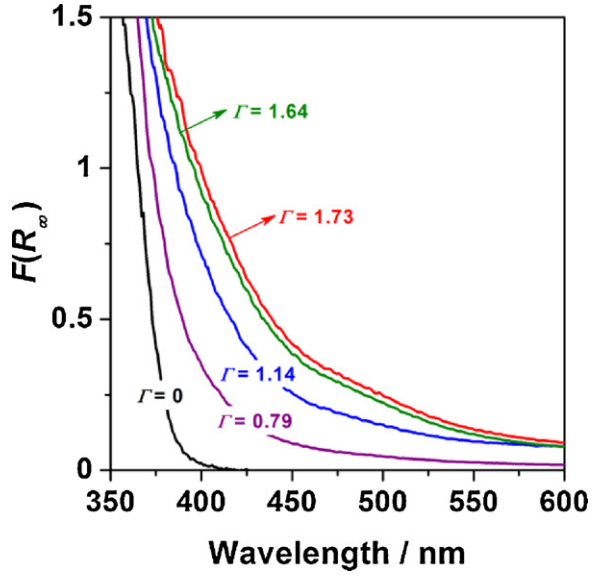

Fig. 7. UV–vis absorption spectra of FeO_x/TiO_2-NTA (U = 40 V, t_a = 1 h, T_c = 873 K) with varying Fe loading amount: $F(R_\infty)$ denotes the Kubelka–Munk function.

absorption intensity of the d–d transition band is very weak at $\Gamma \leq 1.14$ ions nm^{-2}. Evidently, iron oxide clusters can be formed on the TiO_2-NTA surfaces in a highly dispersion state at a molecular level by the CCC technique in a manner similar to the TiO_2 particulate system [22,23].

Fig. 8A shows plots of k_{UV} vs. Γ for the FeO_x/TiO_2-NTA-photocatalzyed degradation of 2-NAP. The iron oxide-surface modification significantly increases the UV-light-activity of TiO_2-NTA at $\Gamma < 1.44$ ions nm^{-2}. The k_{UV} value strongly depends on the Γ, reaching a maximum of 0.72 h^{-1} at Γ = 1.14 ions nm^{-2}. Surprisingly, the value is comparable with that of the highly active P-25 particles (k_{UV} = 1.1 h^{-1}) at the same amount of TiO_2 (7.85 mg/50 mL) in spite that reaction field is highly localized in the film system [22]. We note here that the reactor design for increasing ratio of the TiO_2-NTA to the reaction solution volume should further increase the photocatalytic activity in the film system. Liquid chromatography–mass spectrometry analysis confirmed the formation of phthalic acid and several unidentified intermediates. Fig. 8B shows plots of k_{vis} vs. Γ for the FeO_x/TiO_2-NTA-photocatalzyed degradation of 2-NAP. TiO_2-NTA is almost inactive under illumination of visible-light. Although a visible-light-activity can be induced by fluorine-doping of TiO_2 [35], the fluorine contained in the as-prepared TiO_2-NTA was confirmed to be lost after heating at $T_c > 673$ K by X-ray photoelectron spectroscopy. Interestingly, a significant visible-light-activity is induced by the iron oxide-surface modification with a maximum activity also at Γ = 1.14 ions nm^{-2}. Further, the Fe amount on the TiO_2-NTA surface was confirmed to be invariant at least under the present conditions by ICP spectroscopy. The fact that the highest visible-light- and UV-light-activities are obtained at the same Γ value and the stability of the FeO_x cluster on the TiO_2 surface should be important for the practical use. Photocurrent under illumination of visible light in a Na_2SO_4 aqueous solution has recently been observed for the sulfur-doped TiO_2-NTA electrode; however, no photocatalytic activity data is presented [18].

To gain the information about the unoccupied levels, photoluminescence (PL) spectra were measured. Fig. 9A shows PL spectra of FeO_x/TiO_2-NTA (U = 40 V, t_a = 1 h, T_c) with varying T_c at 77 K: excitation wavelength = 360 nm. As-grown TiO_2-NTA has a weak emission band around 540 nm (E_1) due to the emission from the surface oxygen vacancy levels of TiO_2 [23]. Interestingly, the

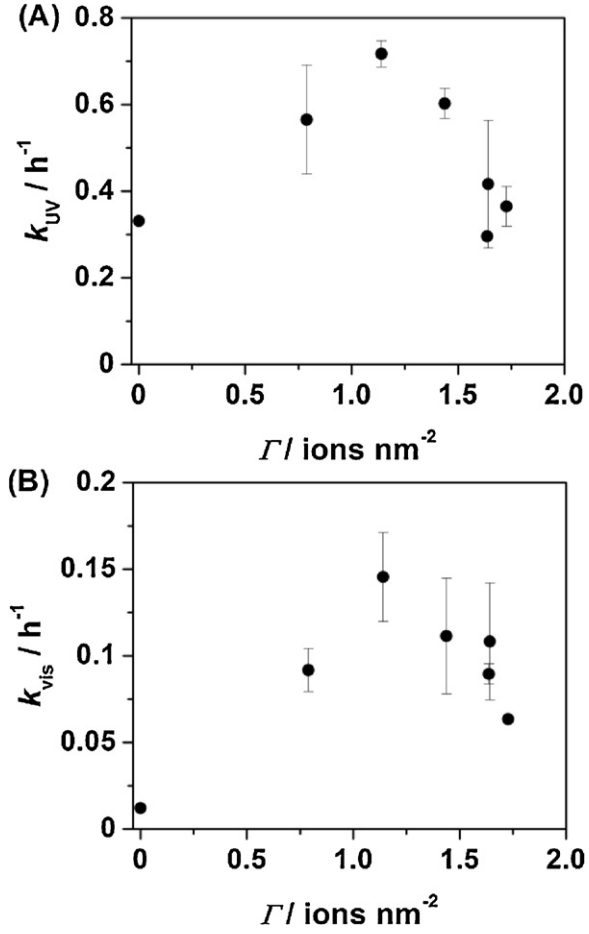

Fig. 8. (A) Plots of k_{UV} vs. x for the FeO_x/TiO_2-NTA-photocatalzyed degradation of 2-NAP. (B) Plots of k_{vis} vs. x for the FeO_x/TiO_2-NTA-photocatalzyed degradation of 2-NAP.

emission intensifies as the T_c increases. This finding suggests that the crystallization and the increase in the crystallinity of TiO_2 increase the diffusion length of the charge carriers. The increase in the probability for the electrons to be trapped at surface vacancy enhances the E_1 emission. At T_c = 973 K, a new emission band (E_2) due to the intrinsic deficiency of rutile TiO_2 appears at 815 nm [36], significantly intensifying at T_c = 1073 K. This result is consistent with the XRD data for the samples with varying T_c. Further, to clarify the action mechanism on the iron oxide-surface modification, the PL spectra were measured for FeO_x/TiO_2-NTA. Fig. 9B shows PL spectra of FeO_x/TiO_2-NTA (U = 40 V, t_a = 1 h, T_c = 873 K) with varying Fe loading amount at 77 K: excitation wavelength = 360 nm. On modifying TiO_2-NTA with the iron oxide species, the intensity of the E_1 band decreases to disappear at Γ = 1.73 ions nm^{-2}, while a new weak emission band appears at 465 nm (E_3). The E_3 signals can be attributed to the emission from the surface iron oxide levels. These findings suggest that the excited electrons in the conduction band (CB) of TiO_2 are transferred to the empty surface iron oxide levels in preference to the surface oxygen vacancy levels. In the oxidative decomposition of organic pollutants, the key to increasing photocatalytic activity of TiO_2 is to enhance the transfer of the excited electrons to O_2 [37,38]. Fig. 10 shows the dark current (I/mA)–potential (E/V vs. Ag/AgCl) curves of the TiO_2-NTA (U = 40 V, t_a = 1 h, T_c = 873 K) electrode and the FeO_x/TiO_2-NTA (U = 40 V, t_a = 1 h, T_c = 873 K) electrode with Γ = 1.14 ions nm^{-2} in a 0.1 M $NaClO_4$ aqueous solution. For the TiO_2-NTA electrode, only small current flows at the potential range between 0 and −0.8 V without O_2 (a), while the current due to the O_2 reduction

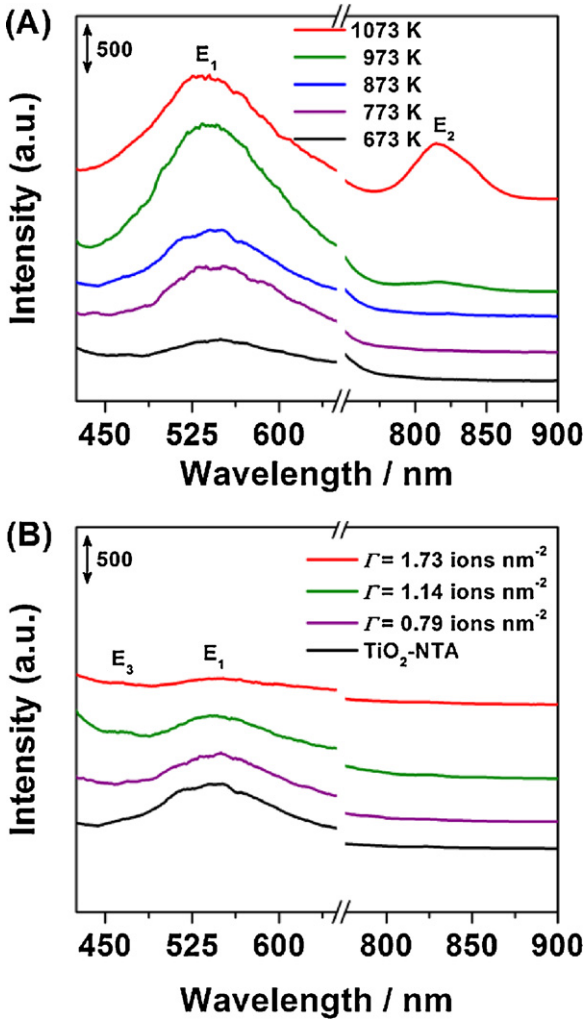

Fig. 9. (A) PL spectra of the TiO_2-NTA (U = 40 V, t_a = 1 h, T_c) with varying T_c. (B) PL spectra of the FeO_x/TiO_2-NTA (U = 40 V, t_a = 1 h, T_c = 873 K) with varying Fe loading amount.

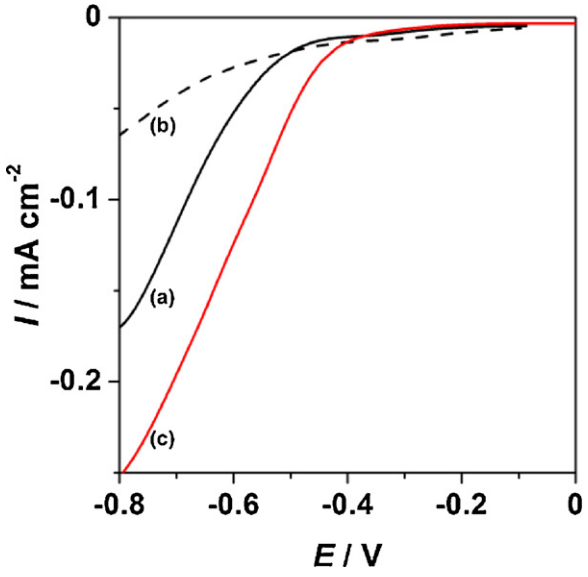

Fig. 10. Dark current–potential curves for the TiO_2-NTA and FeO_x/TiO_2-NTA electrodes: (a) TiO_2-NTA with O_2, (b) TiO_2-NTA without O_2, and (c) FeO_x/TiO_2-NTA with O_2.

is observed at $E < -0.4$ V with O_2 (b). As indicated by curve (c) for the FeO_x/TiO_2-NTA electrode with O_2, the cathodic current is significantly increased by the iron oxide-surface modification. Evidently, the surface iron oxide species drastically promotes the electron transfer from TiO_2 to O_2.

The essential action mechanism of the iron oxide-surface modification of TiO_2 can be explained in a manner similar to the particulate system [23]. Valence band X-ray photoelectron spectroscopic measurements [22] and density functional theory simulation [39,40] have shown that the band gap narrowing of TiO_2 with the iron oxide-surface modification results from the rise in the valence band (VB) top. The visible-light absorption leads to the electronic excitation from the surface *d* sub-band to the conduction band (CB) of TiO_2. On illumination of UV-light, the electrons in the VB(TiO_2) are excited to the CB(TiO_2). In both the cases, without the iron oxide-surface modification, the excited electrons in the CB(TiO_2) are rapidly trapped at the surface oxygen vacancy levels to undergo the recombination with the holes. On the other hand, the iron oxide-surface modification permits the preferential electron transfer from the CB(TiO_2) to the surface iron oxide levels. The electrons effectively reduce adsorbed O_2 by the action of the surface iron oxide species as an excellent mediator. As a result of the effective suppression of the recombination, the photocatalytic activities drastically increase under illumination of visible- and UV-light. A feature of the surface modification in the anodic process should also be stressed that the holes generated in the surface *d* sub-band take part in the oxidation process without diffusion [41]. Meanwhile, the excess loading of the surface iron oxide species would reduce the hole oxidation ability with the rise in the top of the surface *d* sub-band [22], and thus the photocatalytic activity lowers. Consequently, an optimum loading amount is present.

4. Summary

We have shown that the surface modification of TiO_2 nanotube arrays with molecular iron oxide species by the CCC technique endows a high level of visible-light-activity, significantly increasing the UV-light activity. Under optimum conditions, the UV-light-activity is comparable with that of highly active TiO_2 particles. This study should contribute to the development of the supported TiO_2 photocatalyst for environmental purification.

Acknowledgement

This work was supported by a Grant-in-Aid for Scientific Research (B) No. 20350097 from the Ministry of Education, Science, Sport, and Culture, Japan.

References

[1] A. Fujishima, X. Zhang, D.A. Tryk, Surf. Sci. Rep. 63 (2008) 515.
[2] K. Hashimoto, H. Irie, A. Fujishima, Jpn. J. Appl. Phys. 44 (2005) 8269.
[3] S. Ito, S. Inoue, H. Kawada, M. Hara, M. Iwasaki, H. Tada, J. Colloid Interface Sci. 216 (1999) 59.
[4] D. Gong, C.A. Grimes, O.K. Varghese, W. Hu, R.S. Singh, Z. Chen, E.C. Dickey, J. Mater. Res. 16 (2001) 3331.
[5] K. Shankar, G.K. Mor, H.E. Prakasam, S. Yoriya, M. Paulose, O.K. Vargese, C.A. Grimes, Nanotechnology 18 (2007) 065707.
[6] M. Paulose, K. Shankar, S. Yoriya, H.E. Prakasam, O.K. Vargese, G.K. Mor, T.A. Latempa, A. Fitzgerald, C.A. Grimes, Nanotechnology 18 (2007) 065707.
[7] H. Tada, A. Hattori, Y. Tokihisa, K. Imai, N. Tohge, S. Ito, J. Phys. Chem. B 104 (2000) 4585.
[8] H. Chen, S. Chen, X. Quan, H. Yu, H. Zhao, Y. Zhang, J. Phys. Chem. C 112 (2008) 9285.
[9] K. Nakata, B. Liu, Y. Ishikawa, M. Sakai, H. Saito, T. Ochiai, H. Sakai, T. Murakami, M. Abe, K. Takagi, A. Fujishima, Chem. Lett. 40 (2011) 1107.
[10] X. Feng, J.D. Sloppy, T.J. La Tempa, M. Paulose, S. Komarneni, N. Bao, C.A. Grimes, J. Mater. Chem. 21 (2011) 13429.
[11] M. Anpo, M. Takeuchi, J. Catal. 216 (2003) 505.
[12] J. Serpone, N. J. Phys Chem. B 110 (2006) 24287.

[13] H. Zhang, G. Chen, D.W. Bahnemann, J. Mater. Chem. 19 (2009) 5089.
[14] G. Liu, L. Wang, H.G. Yang, H.-M. Cheng, G.Q. Lu, J. Mater. Chem. 20 (2010) 831.
[15] K. Rajeshwar, N.R. de Tacconi, Chem. Soc. Rev. 38 (2009) 1984.
[16] A. Kudo, Y. Miseki, Chem. Soc. Rev. 38 (2009) 253.
[17] X. Chen, S. Shen, L. Guo, S.S. Mao, Chem. Rev. 110 (2010) 6503.
[18] X. Tang, D. Li, J. Phys. Chem. C 112 (2008) 5405.
[19] M. Kitano, K. Funatsu, M. Matsuoka, M. Ueshima, M. Anpo, J. Phys. Chem. B 110 (2006) 25266.
[20] N. Murakami, T. Chiyoya, T. Tsubota, T. Ohno, Appl. Catal. A 348 (2008) 148.
[21] H. Yu, H. Irie, Y. Shimodaira, Y. Hosogi, Y. Kuroda, M. Miyauchi, K. Hashimoto, J. Phys. Chem. C 114 (2010) 16481.
[22] H. Tada, Q. Jin, H. Nishijima, H. Yamamoto, M. Fujishima, S.-i. Okuoka, T. Hattori, Y. Sumida, H. Kobayashi, Angew. Chem. Int. Ed 50 (2011) 3501.
[23] Q. Jin, M. Fujishima, H. Tada, J. Phys. Chem. C 115 (2011) 6478.
[24] Y. Hou, X. Li, X. Zou, X. Quan, G. Chen, Environ. Sci. Technol. 43 (2009) 858.
[25] Y. Shin, S. Lee, Nano Lett. 8 (2008) 3171.
[26] W.H. Hall, Inst. Metals 75 (1950) 1127.
[27] B. Ohtani, Y. Ogawa, S.-i. Nishimoto, J. Phys. Chem. B 101 (1997) 3746.
[28] O.O. Prieto-Mahaney, N. Murakami, R. Abe, B. Ohtani, Chem. Lett. 38 (2009) 238.
[29] A.Y. Ahmed, T.A. Kandiel, T. Oekermann, D. Bahnemann, J. Phys. Chem. Lett. 2 (2011) 2461.
[30] M.I. Litter, J.A. Navio, J. Photochem. Photobiol. A: Chem. 98 (1996) 171.
[31] K. Nagaveni, M.S. Hedge, G. Madras, J. Phys. Chem. B 108 (2004) 20204.
[32] J.A. Navio, G. Colon, M.I. Litter, G.N. Bianco, J. Mol. Catal. A: Chem. 106 (1996) 267.
[33] C.-Y. Wang, D.W. Bahnemann, J.K. Dohrmann, Chem. Commun. (2000) 1539.
[34] N. Serpone, D. Lawless, J. Disdier, J.-M. Hermann, Langmuir 10 (1994) 643.
[35] W. Ho, J.C. Yu, S. Lee, Chem. Commun. (2006) 1115.
[36] J. Shi, J. Chen, Z. Feng, T. Chen, Y. Lian, X. Wang, C. Li, J. Phys. Chem. 111 (2007) 693.
[37] C.M. Wang, A. Heller, H. Gerischer, J. Am. Chem. Soc. 114 (1992) 5230.
[38] M.R. Hoffmann, S.T. Martin, W. Choi, D.W. Bahnemann, Chem. Rev. 95 (1995) 69.
[39] M. Nolan, Phys. Chem. Chem. Phys. 13 (2011) 18194.
[40] M. Nolan, A. Iwaszuk, H. Tada, Aust. J. Chem., in press.
[41] H. Irie, T. Shibanuma, K. Kamiya, S. Miura, T. Yokoyama, K. Hashimoto, Appl. Catal. B 96 (2010) 142.